Supporting Information

An asymmetric wide-bandgap acceptor simultaneously enabling highly efficient single-junction and tandem organic solar cells

Jianqiu Wang,[a,b] Maojie Zhang,*[a] Ji Lin,[a] Zhong Zheng,[a,e] Lei Zhu,[c] Pengqing Bi,[b] Haiyan Liang,[a] Xia Guo,[a] Jingnan Wu,[a] Yafei Wang,[b,f] Linfeng Yu,[a] Jiayao Li,[b,f] Junfang Lv,[a] Xiaoyu Liu,[a,e] Feng Liu,[c] Jianhui Hou[b] and Yongfang Li[a,d,f]

[a] Laboratory of Advanced Optoelectronic Materials, Suzhou Key Laboratory of Novel Semiconductor-optoelectronics Materials and Devices, College of Chemistry, Chemical Engineering and Materials Science, Soochow University, Suzhou 215123, China
E-mail address: mjzhang@suda.edu.cn

[b] State Key Laboratory of Polymer Physics and Chemistry, Beijing National Laboratory for Molecular Sciences, Institute of Chemistry, Chinese Academy of Sciences, Beijing 100190, P. R. China.

[c] Frontiers Science Center for Transformative Molecules, School of Chemistry and Chemical Engineering, Shanghai Jiao Tong University, Shanghai 200240, P. R. China

[d] CAS Key Laboratory of Organic Solids, Beijing National Laboratory for Molecular Sciences, Institute of Chemistry, Chinese Academy of Sciences, Beijing 100190, P. R. China.

[e] School of Chemistry and Biology Engineering University of Science and Technology Beijing, Beijing 100083, China.

[f] University of Chinese Academy of Sciences, Beijing 100049, China

Experimental
Materials

PEDOT:PSS was purchased from Heraeus (*CLEVIOS*TM PVP Al 4083). PM6, BTP-eC9, PFN-Br and PNDIT-F3N-Br were purchased from Solarmer, Inc (Beijing). All solvents used here were commercially available from Acros. ITO coated glass was purchased from South China Xiang's Science & Technical Company. Compound 1 was synthesized according to the reported literature [1] and compound 2 was purchased from Solarmer, Inc (Beijing).

The synthesis of AITC molecular
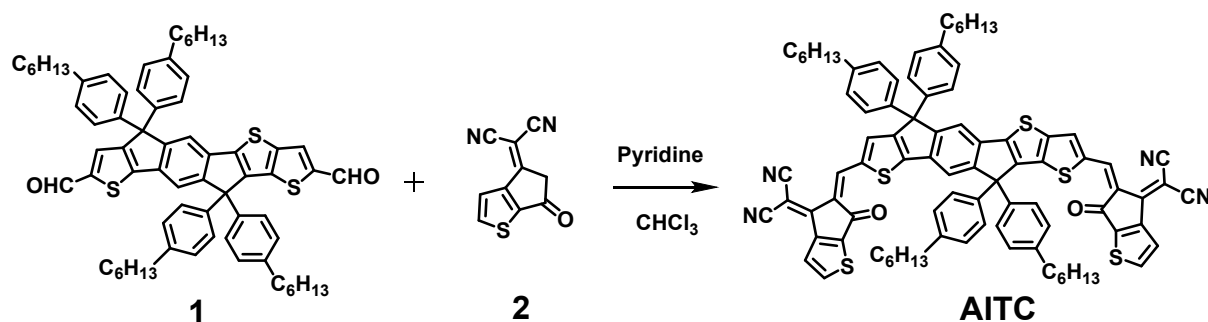
Scheme S1. The synthetic route of AITC.

Compound 1 (199 mg, 0.196 mmol) and compound 2 (117 mg, 0.589 mmol) were dissolved in anhydrous chloroform (30 mL). Pyridine (0.5 mL) was added into the mixtures after being flushed with argon for 5 minutes. Then the reaction mixtures were purged with argon for another 15 minutes. The reaction was stirred at 65°C for 12 h. The product was precipitated in methanol (100 mL) and filtrated. The dried precipitates were purified by silica gel column chromatography by using the mixture of petroleum ether and methylene chloride ($V_{petroleum}$:$V_{methylene}$ = 1:1) to obtain AITC as a dark purple solid (0.19 g, 71%). Then the solid product was recrystallized and dried under vacuum for 24 h before use. ^{1}H NMR (300 MHz, CDCl$_3$) δ 8.62 (s, 2H), 8.13 (s, 1H), 7.96-7.91 (m, 4H), 7.73 (s, 1H), 7.63(s, 1H), 7.55 (s, 1H), 7.20-7.09 (m, 16H), 2.60-2.54 (m, 8H), 1.36-1.26 (m, 32H), 0.88- 0.86 (m, 12H). ^{13}C NMR (75 MHz, CDCl$_3$) δ 180.75, 180.51, 157.72, 157.22, 156.48, 156.30, 156.00, 155.39, 152.45, 152.29, 151.46, 148.39, 147.80, 145.84, 143.34, 142.44, 142.25, 140.53, 140.01, 139.59, 139.38, 139.01, 138.72, 138.44, 137.84, 136.54, 136.26, 135.86, 135.71, 128.85, 128.70, 127.84, 127.74, 125.50, 124.74, 123.50, 119.42, 118.58, 114.17, 113.78, 113.69, 77.45, 77.23, 77.03, 76.60, 69.49, 69.13, 63.17, 62.96, 35.56, 31.70, 31.32, 31.25, 29.15, 29.11, 22.58, 14.10. Elemental analysis calcd (%) for AITC (C$_{88}$H$_{78}$N$_4$O$_2$S$_5$): C=60.02%, H=6.36%, S=5.29%, N=4.17%. MS (MALDI) C$_{88}$H$_{78}$N$_4$O$_2$S$_5$: m/z calc.1383.92, found 1382.1.

Device fabrication and characterization
Device fabrication:

Solution preparation: PEDOT:PSS solution were diluted with the same volume water. PM6:AITC (1:1.2, weight ratio), PM6:BTP-eC9 (1:1.2, weight ratio), and PM6:AITC:BTP-

eC9 (1:0.3:1.2, weight) were dissolved in chlorobenzene, chloroform, chloroform at the polymer concentration of 10 mg ml^{-1}, 8 mg ml^{-1}, and 7.5 mg ml^{-1}, respectively. PNDIT-F3N-Br and PFN-Br were dissolved in methanol at the concentration of 0.5 mg ml^{-1}. All the solutions need to be stirred at 40 °C for at least 4 h. Before spin-coating the active layer, 0.5% 1,8-diiodooctane (v/v) was added to the solutions. ZnO sol-gel solution was prepared through gol-gel method. Zinc acetate dihydrate (100 mg) was dissolved into 1 mL of 2-methoxy ethanol and 27 μL of ethanolamine at room temperature in air. ZnO nano particles (NPs) and ZnO-NPs:PFN-Br solution were prepared according previous literatures.[2-3]

Single-junction OSCs with small area fabrication: The small area OSCs were fabricated by spin coating method. ITO coated glass substrates were cleaned by sonication sequentially in detergent, acetone and isopropanol and then blow-dried by high-purity nitrogen. The ITO substrates were treated in UV-ozone for 15 min, and then diluted PDEOT:PSS solution were spin-coated on top of ITO, and annealed at 160 °C for 10 min under air atmosphere. Afterward, the ITO substrates coated with PEDOT:PSS film were transferred into a nitrogen-purged glove box. The active layer solutions were spin coted onto PEDOT:PSS, and then thermally annealed at 100 °C for 10 min. The 5 nm of PNDIT-F3N-Br was spin-coated on the top of the active layers. Finally, 150 nm of Ag was deposited by thermal evaporation through shadow masks, leading to a defined active area of 0.037 cm^2.

Single-junction rigid OSCs with large area fabrication: The rigid large area OSCs with an inverted structure of Glass/ITO/ZnO/active layer/MoO$_x$/Ag were fabricated by blade coating method. ITO substrates were cleaned by above method. The ZnO sol-gel solution were blade coated onto ITO at a blade rate of 1.5 mm s^{-1}, and blade head height of 20 μm, following by annealing at 200 °C for 30 min. Then, active layer solution with a concentration of 4 mg ml^{-1} was blade coated onto Glass/ITO/ZnO surface. The thickness of active layer films was control to 90-110 nm by adjustment of rate. Subsequently, the substrates containing active layer were transferred into a nitrogen-purged glove box, and annealing 100 °C for 10 min. Finally, the 7nm and 150 nm of MoO$_x$ and Ag were deposited by thermal evaporation. The area of mask is 1.0267 cm^2.

Single-junction flexible OSCs with large area fabrication: The flexible large area OSCs with an inverted structure of PEN/ITO/ZnO/active layer/MoO$_x$/Ag were fabricated by slot-die coating method. PEN/ITO substrates were clean by above method. The ZnO films were obtained by slot-die with the tape speed of 0.2 mm min^{-1}, inking speed of 0.15 ml min^{-1} and slit spacing of 100 μm, following by annealing at 150 °C for 40 min under air atmosphere. Then, active layer solution with a concentration of 3 mg ml^{-1} were slot-die coating onto ZnO surface at the tape speed of 1.0 mm s^{-1}, inking speed of 0.1 ml min^{-1} and slit spacing of 20 μm, following by annealing at 100 °C for 10 min under nitrogen atmosphere. Finally, the 7nm and 150 nm of MoO$_x$ and Ag were deposited by thermal evaporation. The area of mask is 1.0267 cm^2.

Tandem OSCs fabrication: The ZnO layers cast onto Glass /ITO were prepared as described above. Then, PM6:AITC layer was spin-coated, and the spin speed can be tuned to get the blend films with varied thickness. Then 7 nm MoO$_x$ and 0.5 nm ultra-thin Ag layer were evaporated

under high vacuum. Subsequently, the ZnO:PFN-Br solution was casted on the bottom cells and annealed at 110 $^{\circ}$C for 30 min. After that, the solution of PM6:BTP-eC9 was spin-coated to get a varied thick film. Finally, MoO$_x$ and Ag were evaporated on top of top active layer. The cells area as defined by the overlap between the ITO and Ag electrodes, was 0.037 mm^2. The area of the mask is 0.02243 cm^2.

Single carrier devices fabrication: Single-carrier devices contained the same active layers as those in OSCs while different electrodes and charge extraction layers were adopted. The structure of hole and electron only device are ITO /PEDOT:PSS /active layer /Au; ITO /ZnO /active layer /PFN-Br /Ag, respectively.

Instruments and measurements

1H NMR and 13C NMR spectra were collected on a Bruker AVANCE spectrometer with tetramethylsilane (TMS) as the internal standard and CDCl$_3$ as the solvent. Elemental analysis of the polymers was conducted on the Flash EA1112 analyzer. The UV-visible absorption spectra were performed by using a Perkin Elmer General TU-1901 UV-vis spectrophotometer. Grazing incidence X-ray diffraction (GIXD) measurements were performed at beamline 7.3.3 at the Advanced Light Source. The 10 keV X-ray beam was incident at a grazing angle of 0.12°-0.16°, selected to maximize the scattering intensity from the samples. The scattered x-rays were detected using a Dectris Pilatus 2M photon counting detector. The samples for GIXD measurements are fabricated on silicon substrates using the same recipe for the devices. The current density-voltage ($J-V$) tests were carried out under illumination of AM 1.5G 100 mW cm^{-2} using a XES-70S1 (SAN-EI Electric Co., Ltd.) solar simulator (AAA grade) calibrated by a standard single-crystal Si photovoltaic cell (certificated by ational Institute of Metrology). The EQE was measured by a Solar Cell Spectral Response Measurement System QE-R3011 (Enli Technology Co., Ltd. Taiwan). To measure the EQE of bottom and top cell, light bias obtained by 500 nm short wave pass filters and 850 nm long wave pass filters were selected to excite the bottom and top cells, respectively. Photo-CELIV mobilities and TPV data were obtained by the all-in-one characterization platform, Paios (Fluxim AG, Switzerland). Fourier-transform photocurrent spectroscopy external quantum efficiency (EQE$_{FTPS}$) was measured using an integrated system (PECT-600, Enlitech), where the photocurrent was amplified and modulated by a lock-in instrument. EQE$_{EL}$ measurements were performed by applying external voltage/current sources through the devices (ELCT-3010, Enlitech). All of the devices were prepared for EQE$_{EL}$ measurements according to the optimal device fabrication conditions. EQE$_{EL}$ measurements were carried out from 2 to 4 V, and then luminous spectra with a wavelength range of 400-1100 nm were collected by a high resolution and highly sensitive back-illumination CCD detection array.

The stability measurements of the OPV cells.

The OPV cells were encapsulated with UV curing adhesive, which were then irradiated under a 365 nm UV lamp for 15 min. The stability of the encapsulated OPV cells were measured in air under continuous LED lamp with 1 sun-equivalent illumination. The light intensity calibrated by matching the device performance to those measured under AM1.5 G, 100 mW cm^{-2}. The temperature is about 55 °C and the relative humidity is about 40%.

Determinations of energy level

The HOMO and LUMO energies were determined by electrochemical method. We provide more detailed experimental processes and calculation methods. Cyclic voltammetry (CV) was performed on a Zahner Zennium IM6 electrochemical workstation with a three-electrode system in 0.1 mol L^{-1} Bu_4NPF_6 acetonitrile solutions at a scan rate of 50 mV s^{-1}. The three-electrode system included glassy carbon disk, platinum wire and Ag/Ag^+ electrode as the working electrode, counter electrode and reference electrode, respectively. The potential of the Ag/Ag^+ reference electrode was internally calibrated by using the ferrocene/ferrocenium redox couple (Fc/Fc^+), and the Ag/Ag^+ reference electrode possesses an energy level of 4.80 eV. Therefore, HOMO and LUMO are obtained according to the equations: HOMO = $-e(\varphi_{ox} + 4.80 - \varphi_{Fc/Fc+})$ (eV) and LUMO = $-e(\varphi_{re} + 4.80 - \varphi_{Fc/Fc+})$ (eV), where φ_{ox} and φ_{re} are onset oxidation potential and onset reduction potential, respectively.

Determinations of absorption coefficient

The absorption coefficient is calculated based on the equation:

$$Abs = \frac{-lg\frac{I}{I_0}}{} \quad \text{Equation S1}$$

$$\frac{\alpha}{L} = -ln\frac{I}{I_0} \quad \text{Equation S2}$$

where I, I_0, α and L are transmission light, intensity incident light intensity, absorption coefficient and film thickness, respectively. The absorbance is measured by UV-vis spectrometer. The thickness the films are controlled to 30 nm.

Determinations of charge mobility

The single carrier mobility was determined by fitting the dark *J-V* curve of single carrier devices using Mott–Gurney formula:

$$J = \frac{9}{8}\varepsilon_0\varepsilon_r\mu_{h(e)}\frac{(V - V_{bi})^2}{L^3} \quad \text{Equation S3}$$

where ε_0 and ε_r are the dielectric constant ($\varepsilon_r = 3.5$) of the BHJ layer, $\mu_{h(e)}$ is the hole (or electron) mobility, V_{bi} is the built-in voltage arising from the electrode work function offset, and *L* is the film thickness of photoactive layer.

The bulk carrier mobility is calculated by Equation S4:

$$\mu = \frac{2d^2}{3At_{max}^2(1 + 0.36\Delta j/j_0)} \quad \text{Equation S4}$$

where *d*, *A*, t_{max}, j_0 are film thickness, the voltage rises speed of the applied voltage pulse, the time to reach the extraction current maximum, respectively. The j_0 arising from the geometrical capacitance of the sample, given as

$$j_0 = \frac{\varepsilon\varepsilon_0 A}{d} \quad \text{Equation S5}$$

where ε and ε_0 are where ε_0 and ε_r is the dielectric constant ($\varepsilon_r = 3.5$) of the BHJ layer, respectively.

Determinations of energy losses

The voltage losses in photovoltage cell can be categorized into three contributions:

$$\Delta V = \frac{E_g}{q} - V_{oc} = (\frac{E_g}{q} - V_{OC}^{SQ}) + (V_{OC}^{SQ} - V_{OC}^{rad}) + (V_{OC}^{rad} - V_{OC}) = \Delta E1 + \Delta E2 + \Delta E3 \quad \text{Equation S6}$$

E_g is the optical gap determined from intersection point of normalized EQE and EL spectra. V_{OC}^{SQ} is the maximum voltage based in the Shockley-Queisser (SQ) limit, where the EQE_{PV} is assumed to be a step-function, i.e., 1 above the gap and 0 below the gap. In SQ limit, V_{OC}^{SQ} follows

$$V_{OC}^{SQ} = \frac{KT}{q}\ln\left(\frac{J_{SC,SQ}}{J_{0,SQ}} + 1\right) = \frac{KT}{q}\ln\left(\frac{q\int_{Eg}^{\infty}\emptyset_{AM1.5}(E)dE}{q\int_{Eg}^{\infty}\emptyset_{bb}(E)dE} + 1\right) \quad \text{Equation S7}$$

where $\emptyset_{AM1.5}$ is the solar radiation photo flux, $\emptyset_{bb}$ is a black body radiation at 300K. V_{OC}^{rad} is the voltage where the all recombination is radiative (i.e., $EQE_{EL}=1$), and follows from

$$V_{OC}^{rad} = \frac{KT}{q}\ln\left(\frac{J_{SC,rad}}{J_{0,rad}} + 1\right) = \frac{KT}{q}\ln\left(\frac{q\int_{Eg}^{\infty}EQE_{PV}\emptyset_{AM1.5}(E)dE}{q\int_{Eg}^{\infty}EQE_{PV}\emptyset_{bb}(E)dE} + 1\right) \quad \text{Equation S8}$$

The voltage loss due to non-radiative recombination can be obtained by:

$$\Delta V_{OC}^{non-rad} = V_{OC}^{rad} - V_{OC} \quad \text{Equation S9}$$
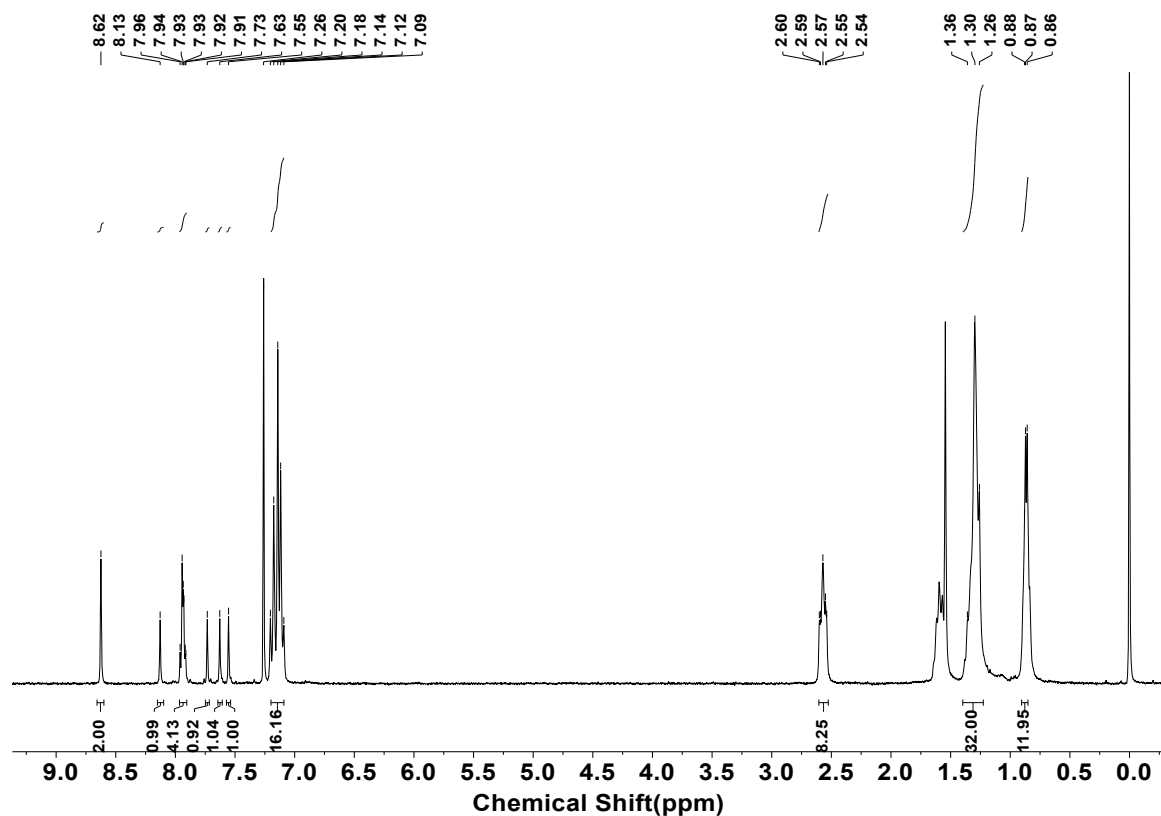
Figure S1. ^{1}H NMR spectra of AITC.
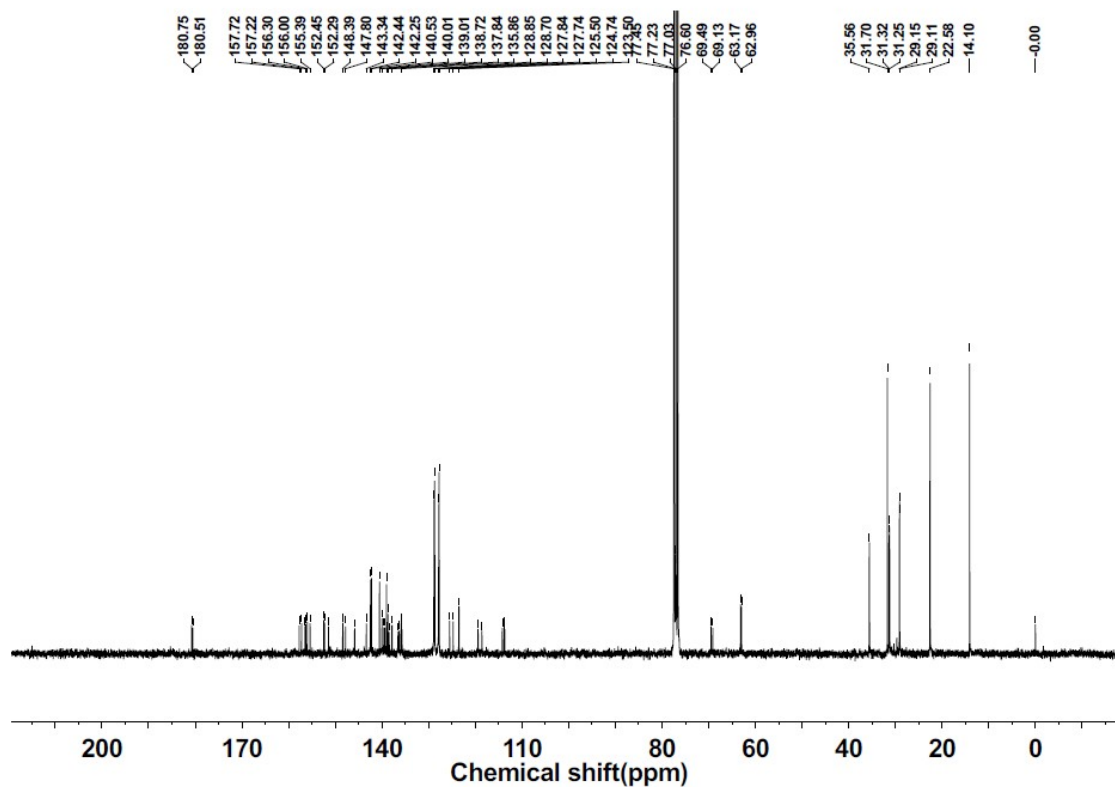
Figure S2. ^{13}C NMR spectra of AITC.
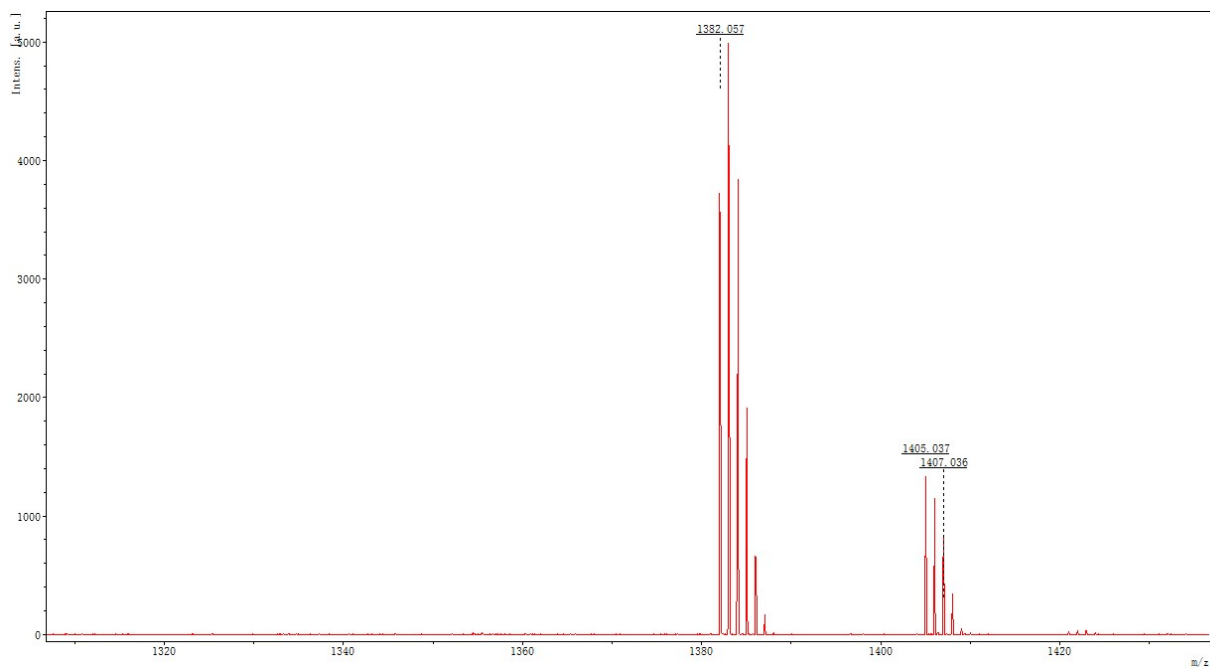
Figure S3. MALDI-TOF spectra of AITC.
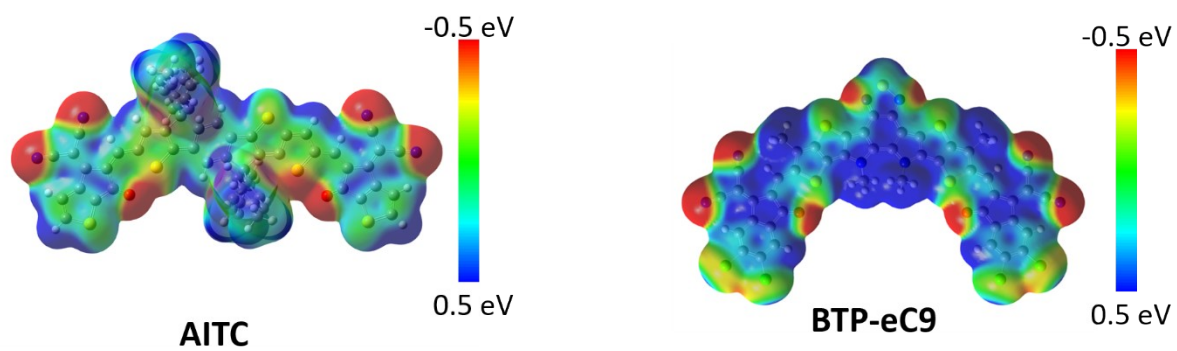
Figure S4. Electrostatic potential (ESP) maps of AITC and BTP-eC9 molecular. The high ESP values suggest their excellent electron-accepting capacity.
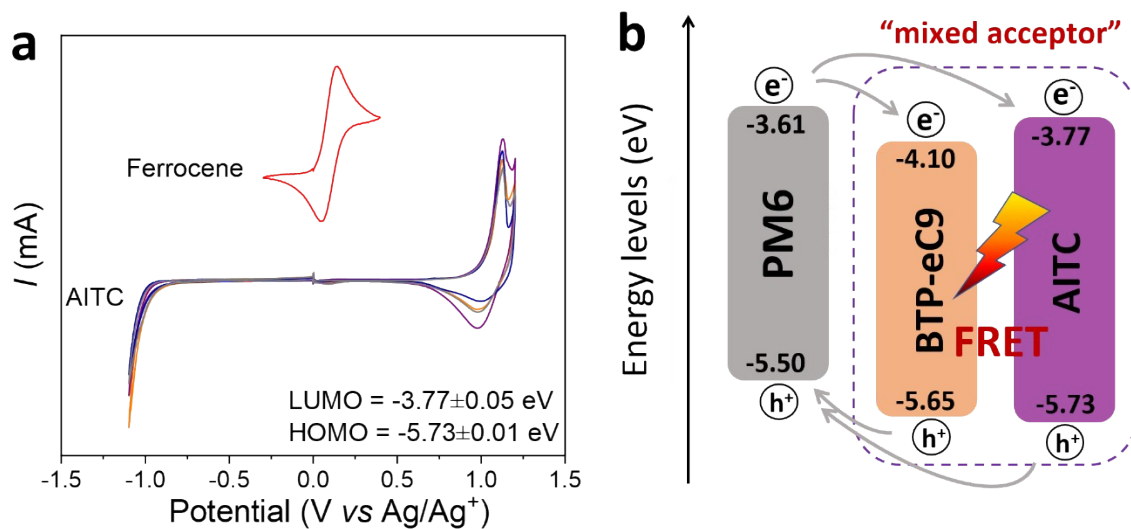
Figure S5. a) Cyclic voltammetry (CV) plots of AITC. Inset show the estimated energy levels. b) The energy level of all materials.
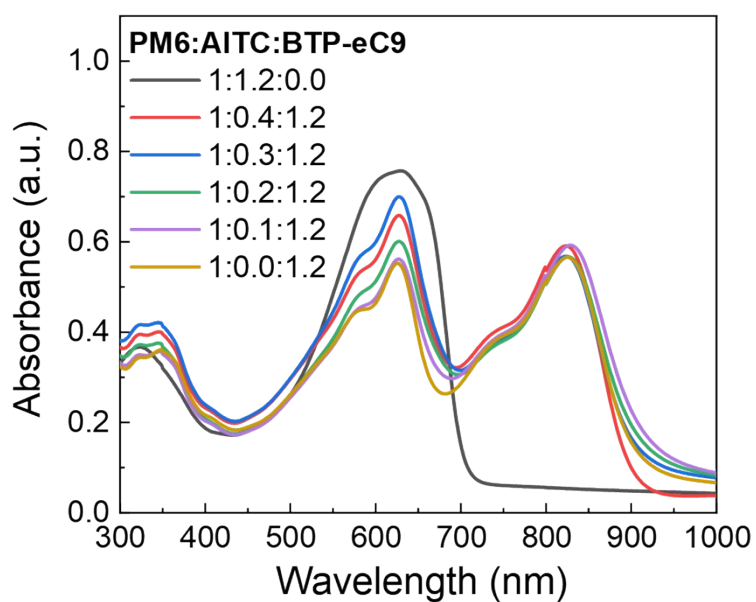
Figure S6. The absorption spectra of PM6:AITC:BTP-eC9 blend film with different weight ratios.
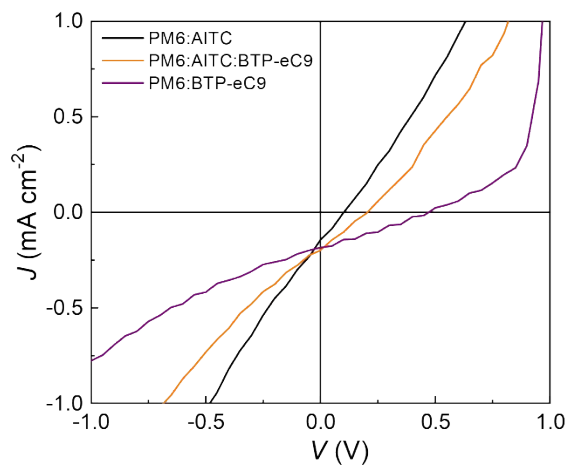
Figure S7. *J-V* curves of OSCs based AITC, BTP-eC9 and AITC:BTP-eC9 films.

Table S1. Photovoltaic parameters of AICT, BTP-eC9 and AITC:BTP-eC9 based OSCs.

OSCs	V_{OC} (V)	J_{SC} (mA cm^{-2})	FF (%)	PCE (%)
AICT	0.102	0.143	29.30	0.004
ITC:BTP-eC9	0.205	0.198	25.52	0.010
BTP-eC9	0.472	0.185	29.71	0.031
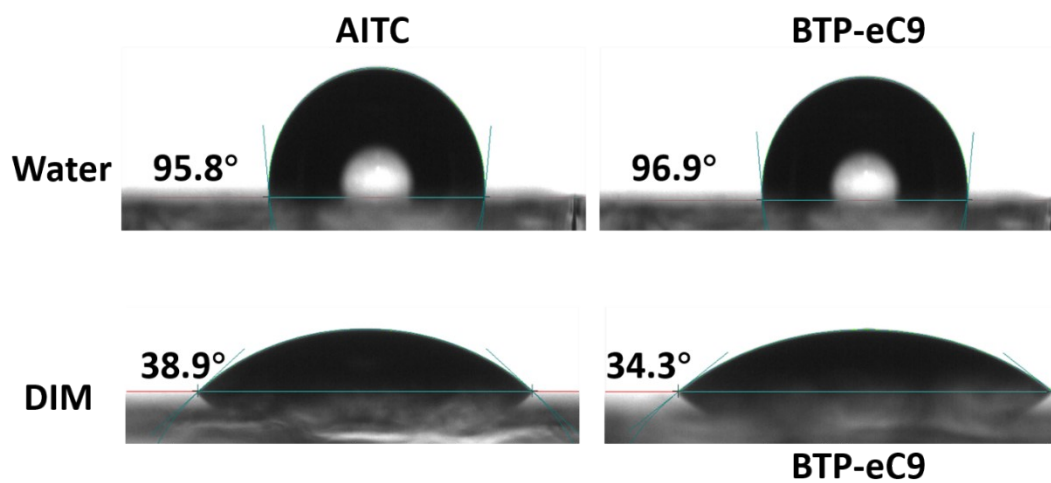
Figure S8. The contact angle of water and diiodomethane (DIM) on two films.
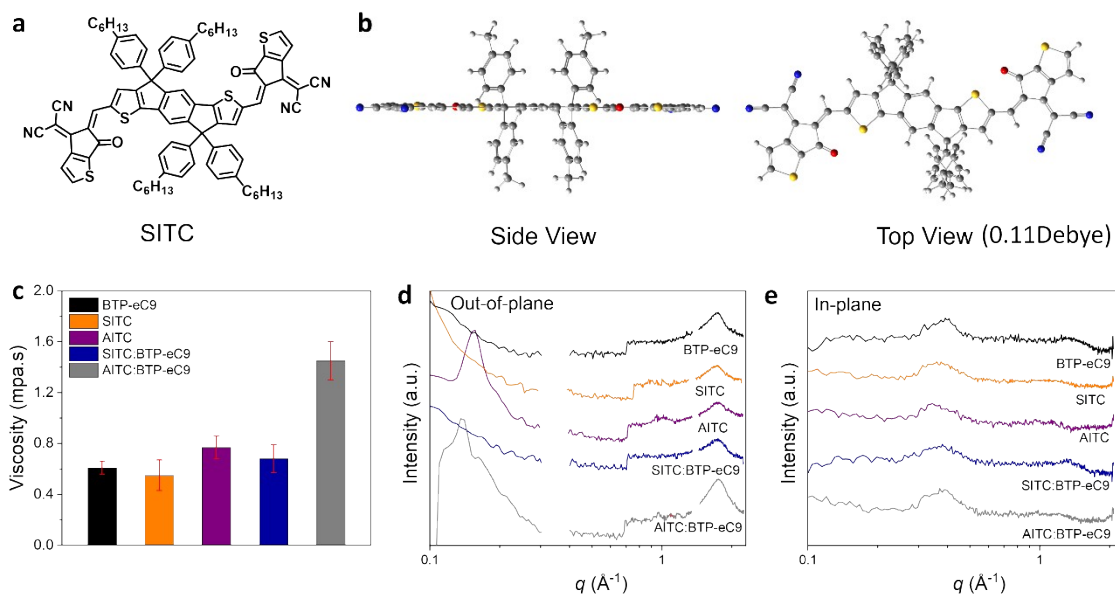
Figure S9. a) The molecular structure and b) calculated geometries of SITC. c) The viscosity of five precursor solutions. All the materials are dissolved in chloroform solvent at the concentration of 10 mg ml^{-1}. GIWAXS cut-line profiles of five films in c) out-of-plane and d) in-plane direction.

Table S2. Detailed GIWAXS (010) peak information of three BHJ films.

BHJ	q (Å^{-1})	d-spacing (Å)	FWHM (Å^{-1})	CCL (Å)
PM6:AITC	1.76	3.57	0.273	20.69
PM6:AITC:BTP-eC9	1.74	3.61	0.269	21.00
PM6:BTP-eC9	1.73	3.63	0.272	20.78
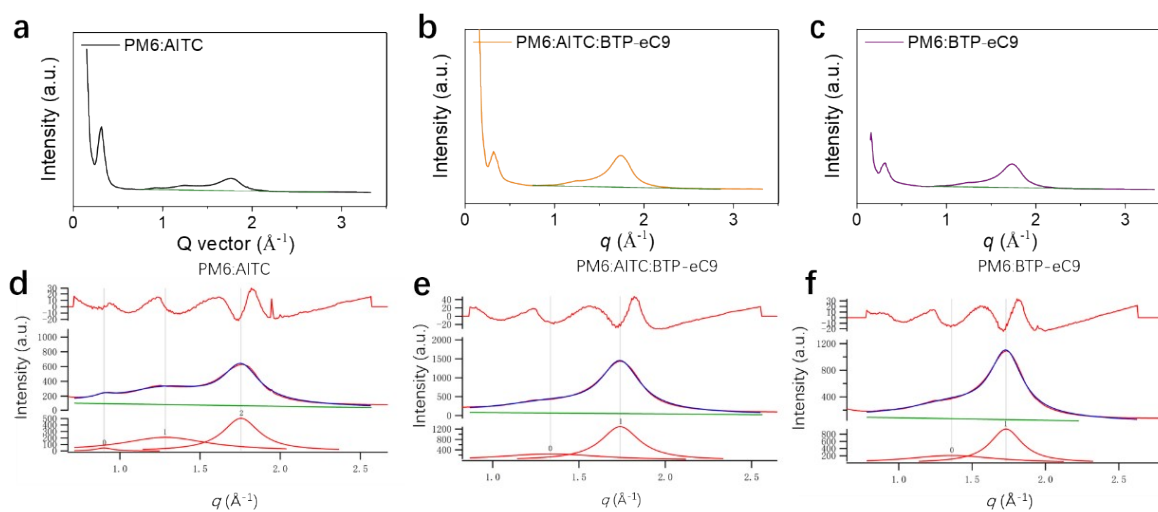
Figure S10. a-c) Line-cut profiles in the out-of-plane directions of three BHJ films. The green line is the baseline. d-f) The results of peak differentiating (bottom), cumulative fit peak (middle) and error (top), respectively. In the middle of figure, the blue and red curves are fitting

and initial data, respectively. The subtract baseline of measured data before calculate the FWHM of peak. Firstly, the baseline of peak near $q=1.75$ Å^{-1} are established by the linear mode. In linear coordinates, the starting- and ending- point of the baseline are the lowest point on either side of the peak, as shown in **Figure S10a-c**. Secondly, the Gaussian functions are employed to differentiate the peaks. The differentiated peaks and cumulative fit peak results are shown in **Figure S10d-f**. In differentiating of the peak, the peak position is fixed, which corresponds to the peak (010) position. Then, the FWHM and area are obtained. The information about the size of crystalline grains is contained in the FWHM of the diffraction peaks, and it can be expressed by the Scherrer equation, CCL = $0.9 \times 2\pi/(\Delta q)$, which gives an approximation of the grain size.
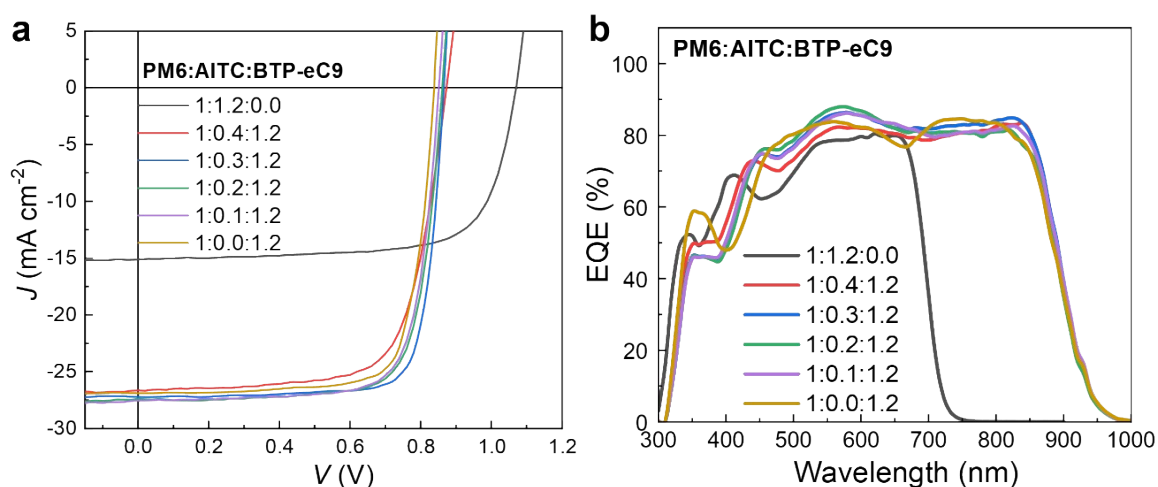
Figure S11. a) *J-V* curves and b) EQE spectrum of OSCs based on PM6:AITC:BTP-eC9 BHJ with various ratio of donor and acceptor.

Table S3. Photovoltaic parameters of PM6:AITC:BTP-eC9 based solar cell with different D/A ratios.

PM6:AITC:BTP-eC9	V_{OC} (V)	J_{SC}/J_{cal} (mA cm^{-2})[a]	FF (%)	PCE (%)
1:1.2:0.0	1.07	14.3/14.2	71.6	11.0
1:0.4:1.2	0.87	26.6/26.0	70.5	16.4
1:0.3:1.2	0.87	27.2/26.7	79.7	18.8
1:0.2:1.2	0.86	27.4/26.3	76.4	18.0
1:0.1:1.2	0.85	27.6/26.4	75.9	17.8
1:0.0:1.2	0.84	26.9/26.1	76.5	17.2

[a]Integrated J_{cal} in parenthesis from the EQE curves.

Table S4. Summary of some representative ternary OSCs with PCEs of over 18%.

BHJ	V_{OC} (V)	J_{SC} (mA cm^{-2})	FF (%)	PCE (%)	Ref
PBDB-TF:HDO-4Cl:eC9	0.866	27.05	80.51	18.86	4

PBQx-TF:eC9-2Cl:F-BTA3	0.879	26.7	80.9	19.0	5
D18-Cl:G19:Y6	0.871	27.36	77.72	18.53	6
PM6:BTP-eC9:L8-BO-F	0.853	27.35	80.0	18.66	7
PM6:BTP-eC9:BTP-F	0.858	26.99	79.7	18.45	8
PBDB-TF:PB2F:BTP-eC9	0.863	26.8	80.4	18.6	9
PTQ10:m-BTP-PhC6:PC$_{71}$BM	0.869	26.99	80.6	18.89	10
PM6:PM6-Si30:C9	0.870	26.90	78.04	18.27	11
PM6:ITIC-M:Y6	0.859	26.35	80.10	18.13	12
PM6:AITC:BTP-eC9	0.87	27.2	79.7	18.8	This study
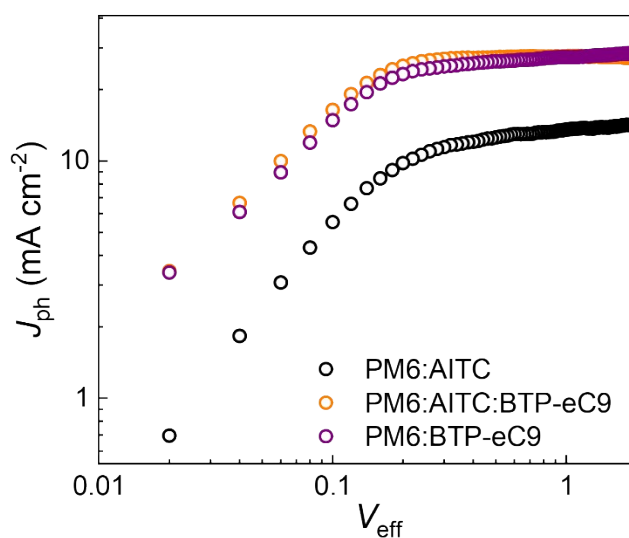
Figure S12. The J_{ph}-V_{eff} curves of the cells based on various BHJ.

Table S5. The exciton dissociation probabilities of solar cells with different BHJs.

BHJ	P_{diss} (%)[a]
PM6:AITC	95
PM6:AITC:BTP-eC9	99
PM6:BTP-eC9	96

[a]The exciton dissociation probabilities.
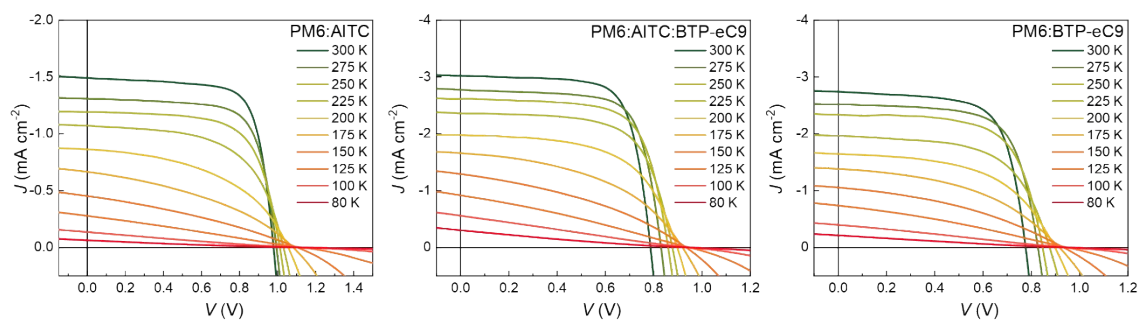
Figure S13. *J-V* curves of the three OSCs at various temperature under AM 1.5G, 10 mW cm⁻².
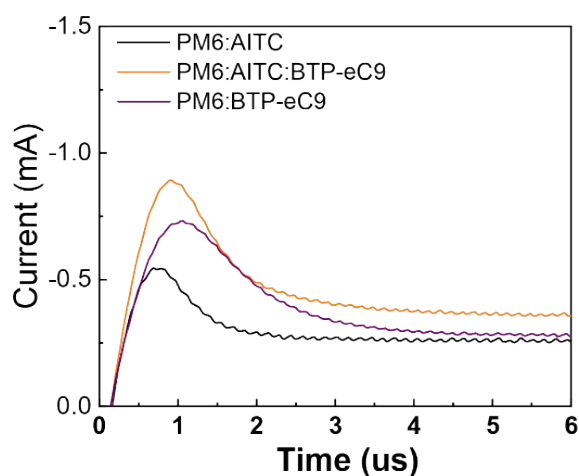
Figure S14. Photo-CELIV curves of three OSCs. The ramp rate is 316 V/ms.
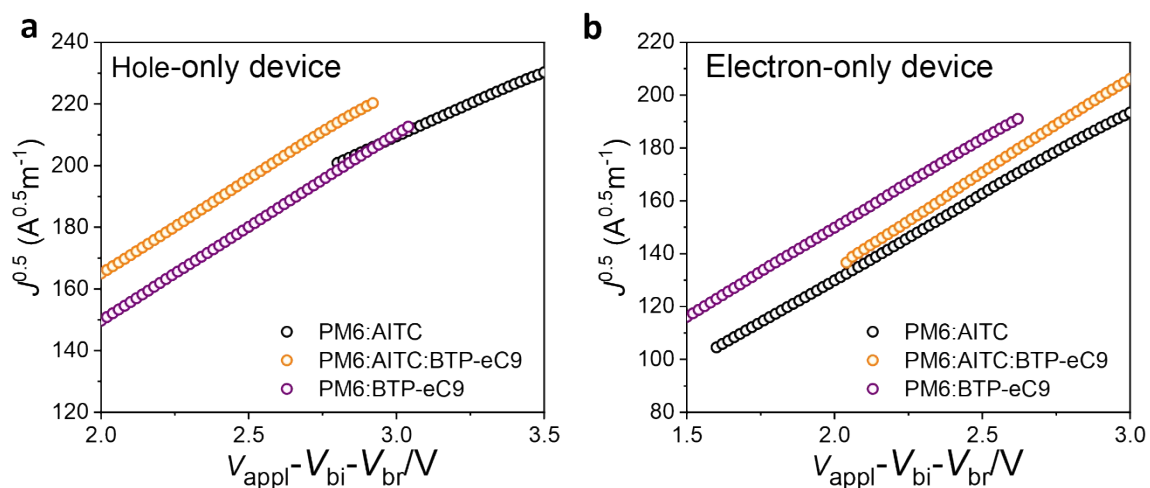
Figure S15. Dark *J-V* curves of a) hole-only and b) electron-only devices containing different BHJ.

Table S6. The mobility of blend films.

BHJ	μ_h [cm^2 V^{-1} s^{-1}]	μ_e [cm^2 V^{-1} s^{-1}]	μ_h/μ_e[a]
PM6:AITC	3.63×10^{-4}	5.01×10^{-4}	0.72
PM6:AITC:BTP-eC9	8.49×10^{-4}	8.79×10^{-4}	0.97
PM6:BTP-eC9	6.17×10^{-4}	6.61×10^{-4}	0.93

[a]Mobility ratio between hole and electron.
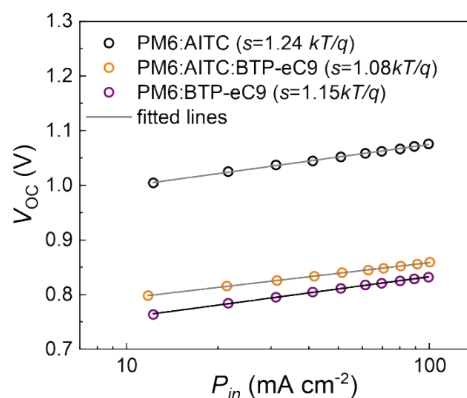
Figure S16. V_{OC} versus light intensity (P_{in}) characteristics of binary and ternary OSCs.
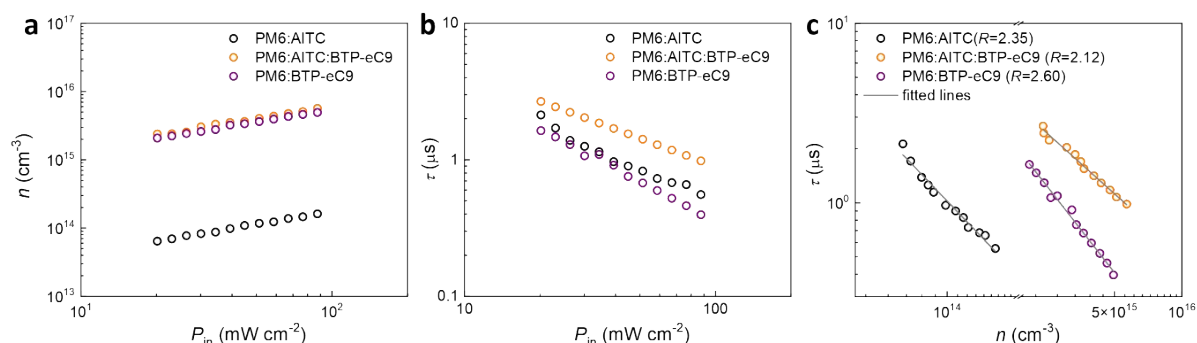
Figure S17. a) charge carrier density (n) and b) charge carrier lifetime (τ) under various light intensity. c) τ as a function of n in three OSCs.

Table S7. Detailed energy losses of the three OSCs.

OSCs	E_g[a] (eV)	qV_{OC} (eV)	qV_{loss} (eV)	$\Delta E1$ (eV)	$\Delta E2$ (eV)	$\Delta E3$ (eV)	$\Delta E3$[b] (eV)
PM6:AITC	1.80	1.07	0.73	0.29	0.10	0.32	0.30
PM6:AITC:BTP-eC9	1.40	0.87	0.53	0.26	0.06	0.21	0.22
PM6: BTP-eC9	1.40	0.84	0.56	0.26	0.06	0.24	0.24

[a]E_{gap} is the optical bandgap of the film calculated on the basis of the intersections between the normalized absorption and EL spectra of films. [b]$\Delta E3$ is calculated from the EQE$_{EL}$

measurements.
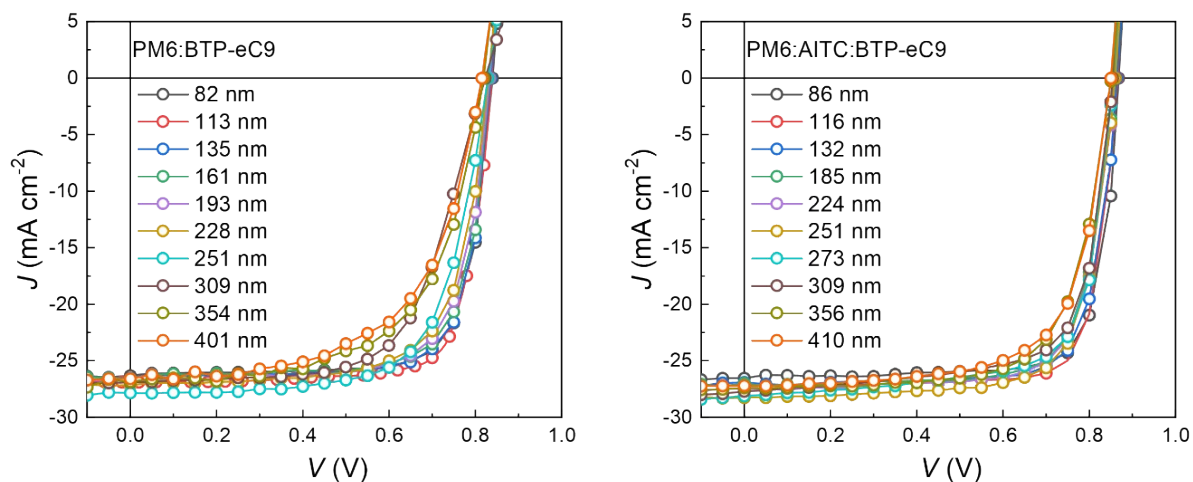
Figure S18. *J-V* curves of OSCs based on PM6:BTP-eC9 and PM6:AITC:BTP-eC9 active layer with various thickness.

Table S8. The photovoltaic performance of OSCs with various thickness of active layers under AM 1.5G, 100mW cm^{-2}.

BHJ	Thickness (nm)	V_{OC} (V)	J_{SC} (mA cm^{-2})	FF (%)	PCE (%)
PM6:BTP-eC9	82	0.84	26.3	77.1	17.0
	113	0.84	27.3	76.5	17.5
	135	0.84	26.5	75.7	16.8
	161	0.83	26.6	74.5	16.5
	193	0.83	26.8	72.2	16.1
	228	0.83	27.2	69.9	15.7
	251	0.83	27.9	68.1	15.7
	309	0.82	26.9	63.9	14.2
	354	0.82	26.8	61.2	13.5
	401	0.82	26.6	60.1	13.0
PM6:AITC:BTP-eC9	86	0.87	26.5	79.6	18.3
	116	0.87	27.2	79.6	18.8
	132	0.86	26.9	78.8	18.3
	185	0.86	27.0	76.6	17.8
	224	0.86	27.5	75.7	17.9
	251	0.86	28.3	74.5	18.1
	273	0.86	28.1	72.6	17.5
	309	0.85	27.7	71.6	16.8

| 356 | 0.85 | 27.6 | 70.3 | 16.5 |
| 410 | 0.85 | 27.2 | 68.8 | 15.9 |
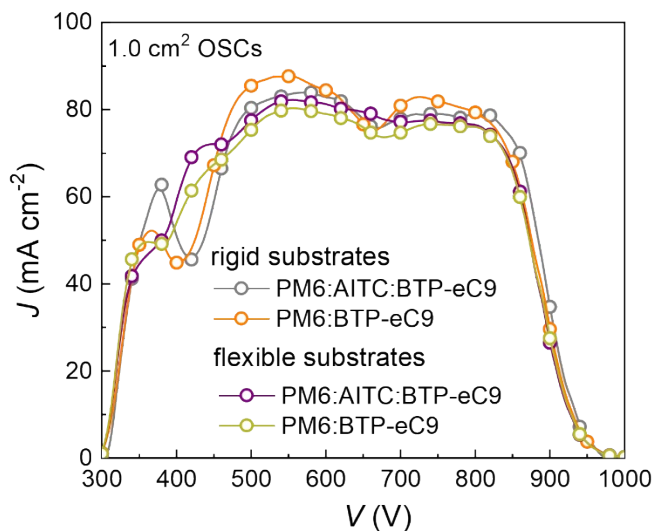
Figure S19. EQE spectrum of 1.0 cm^2 rigid and flexible OSCs.
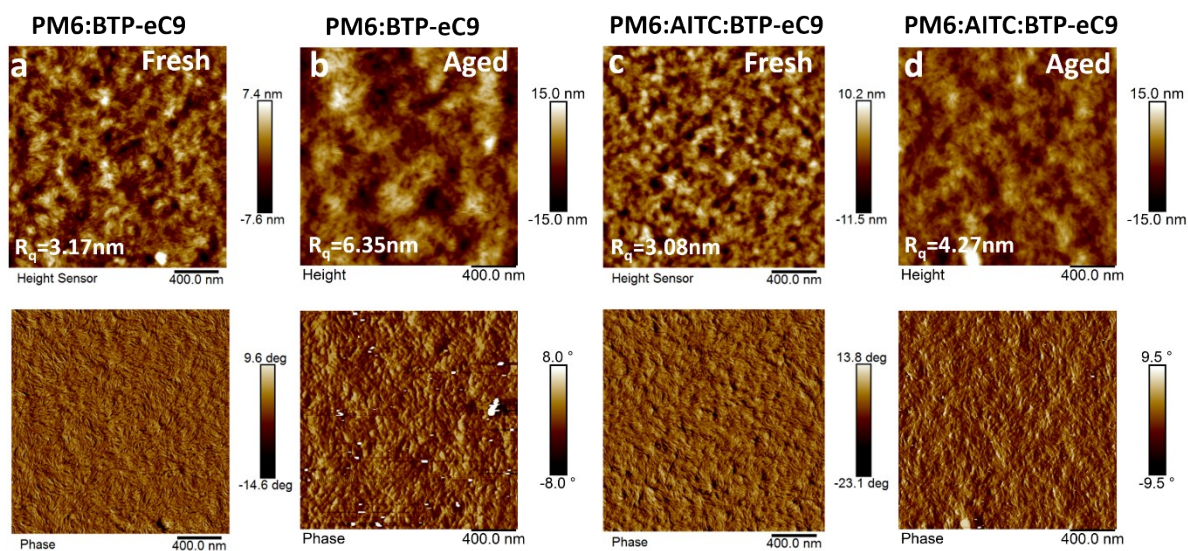
Figure S20. The AFM images of fresh and aged films of a,b) PM6:BTP-eC9 and c,d) PM6:AITC:BTP-eC9. The aged films are illumination along with heating at 100 °C for 500 h.

Table S9. Summary of some representative tandem OSCs.

Bottom	Top	V_{OC} (V)	J_{SC} (mA cm^{-2})	FF (%)	PCE (%)	Ref
PBDB-TF:GS-ISO	PBDB-TF:BTP-eC9	2.01	13.14	76.75	20.27	13
PBDB-TF:ITCC	PBDB-TF:BTP-eC11	1.91	14.21	72.37	19.64	14
PBDB-TF:GS-ISO	PBDB-TF:BTP-eC9	2.03	12.86	73.16	19.10	15

PM7:TfIF-4Cl	PCE10:COi8DFIC:PC$_{71}$BM	1.64	14.59	78	18.71	16
PTQ10: *m*-DTC-2Cl	PTB7-Th: BTPV-4F-eC9	1.621	14.65	70.20	16.67	17
PM6:*m*-DTC-2F	PTB7-Th:BTPV-4F:PC$_{71}$BM	1.65	14.5	68.5	16.4	18
PBDB-T:F-M	PTB7-Th:O6T-4F:PC$_{71}$BM	1.636	14.35	73.7	17.36	19
PM6:AITC	PM6:AITC:BTP-eC9	1.92	13.6	74.6	19.4	This study

References

[1] W. Gao, M. Zhang, T. Liu, R. Ming, Q. An, K. Wu, D. Xie, Z. Luo, C. Zhong, F. Liu, F. Zhang, H. Yan, C. Yang, *Adv. Mater.* 2018, **30**, 1800052.

[2] W. J. E. Beek, M. M. Wienk, M. Kemerink, X. Yang, R. A. J. Janssen, *J. Phys. Chem. B* 2005, **109**, 9505.

[3] Z. Zheng, S. Zhang, J. Wang, J. Zhang, D. Zhang, Y. Zhang, Z. Wei, Z. Tang, J. Hou, H. Zhou, *J. Mater. Chem. A* 2019, **7**, 3570.

[4] P. Bi, S. Zhang, Z. Chen, Y. Xu, Y. Cui, T. Zhang, J. Ren, J. Qin, L. Hong, X. Hao and J. Hou, *Joule*, 2021, **5**, 2408-2419.

[5] Y. Cui, Y. Xu, H. Yao, P. Bi, L. Hong, J. Zhang, Y. Zu, T. Zhang, J. Qin, J. Ren, Z. Chen, C. He, X. Hao, Z. Wei and J. Hou, *Adv. Mater.*, 2021, **33**, 2102420.

[6] Z. Chen, W. Song, K. Yu, J. Ge, J. Zhang, L. Xie, R. Peng and Z. Ge, *Joule*, 2021, **5**, 2395-2407.

[7] Y. Cai, Y. Li, R. Wang, H. Wu, Z. Chen, J. Zhang, Z. Ma, X. Hao, Y. Zhao, C. Zhang, F. Huang and Y. Sun, *Adv. Mater.*, 2021, **33**, 2101733.

[8] Y. Li, Y. Cai, Y. Xie, J. Song, H. Wu, Z. Tang, J. Zhang, F. Huang and Y. Sun, *Energy Environ. Sci.*, 2021, **14**, 5009-5016.

[9] T. Zhang, C. An, P. Bi, Q. Lv, J. Qin, L. Hong, Y. Cui, S. Zhang and J. Hou, *Adv. Energy Mater.*, 2021, **11**, 2101705.

[10] S. Bao, H. Yang, H. Fan, J. Zhang, Z. Wei, C. Cui and Y. Li, *Adv. Mater.*, 2021, **33**, 2105301.

[11] W. Peng, Y. Lin, S. Y. Jeong, Z. Genene, A. Magomedov, H. Y. Woo, C. Chen, W. Wahyudi, Q. Tao, J. Deng, Y. Han, V. Getautis, W. Zhu, T. D. Anthopoulos and E. Wang, *Nano Energy*, 2022, **92**, 106681.

[12] Y. Zeng, D. Li, H. Wu, Z. Chen, S. Leng, T. Hao, S. Xiong, Q. Xue, Z. Ma, H. Zhu and Q. Bao, *Adv. Funct. Mater.*, 2021, DIO:10.1002/adfm.202110743.

[13] Z. Zheng, J. Wang, P. Bi, J. Ren, Y. Wang, Y. Yang, X. Liu, S. Zhang and J. Hou, *Joule*, 2021, DOI:10.1016/j.joule.2021.12.017.

[14] P. Bi, S. Zhang, J. Ren, Z. Chen, Z. Zheng, Y. Cui, J. Wang, S. Wang, T. Zhang, J. Li, Y. Xu, J. Qin, C. An, W. Ma, X. Hao and J. Hou, *Adv. Mater.*, 2021, DIO:10.1002/adma.202108090.

[15] J. Wang, Z. Zheng, Y. Zu, Y. Wang, X. Liu, S. Zhang, M. Zhang and J. Hou, *Adv. Mater.*, 2021, **33**, 2102787.

[16] G. Liu, R. Xia, Q. Huang, K. Zhang, Z. Hu, T. Jia, X. Liu, H. L. Yip and F. Huang, *Adv. Funct. Mater.*, 2021, **31**, 2103283.

[17] Z. Jia, S. Qin, L. Meng, Q. Ma, I. Angunawela, J. Zhang, X. Li, Y. He, W. Lai, N. Li, H. Ade, C. J. Brabec and Y. Li, *Nat. Commun.* 2021, **12**, 178.

[18] S. Qin, Z. Jia, L. Meng, C. Zhu, W. Lai, J. Zhang, W. Huang, C. Sun, B. Qiu and Y. Li, *Adv. Funct. Mater.* 2021, **31**, 2102361.

[19] L. Meng, Y. Zhang, X. Wan, C. Li, X. Zhang, Y. Wang, X. Ke, Z. Xiao, L. Ding, R. Xia, H.-L. Yip, Y. Cao and Y. Chen, *Science*, 2018, **361**, 1094-1098.